Dynamic Power Convertor Validation and Verification Thermal Analysis

Terry V. Reid[1] and Scott D. Wilson[2]
NASA Glenn Research Center, Cleveland, OH, 44135, USA

Matthew Stang[3]
NASA Glenn Research Center, Cleveland, OH, 44135, USA

NASA Glenn Research Center is preparing to perform experimental testing on various Stirling Convertors in the < 100-watt range. Prior to testing, a variety of computational simulations are being performed with the convertors-only (in isolation), and with the convertors equipped with an anticipated insulation and heating package that will be part of experimental test article. The goal is to develop a calculation methodology that will assist in predicting the convertor parasitic losses as well as estimating convertor efficiency. Three different cold-end temperatures will be explored on two different convertors, and the contribution of radiation within the heater head itself was included.

I. Nomenclature

e	=	$\varepsilon + u^2/2$; mass-specific total gas energy
$\boldsymbol{n}$	=	unit outward normal of s
$\boldsymbol{q}$	=	heat flux vector
s	=	surface of v
t	=	time
v	=	control volume
$\boldsymbol{V}$	=	Newtonian-frame flow velocity vector
$\boldsymbol{V_r}$	=	boundary-relative flow velocity vector
ε	=	mass-specific internal gas energy
ρ	=	gas density
$\boldsymbol{\sigma}$	=	stress tensor
GHI	=	Gross Heat Input
NHI	=	Net Heat Input
$\dot{Q}$	=	Rate of heat transfer
T	=	Temperature
CE	=	Cold-end
HE	=	Hot-end
HS	=	Heat Source
ES	=	Expansion space
ENV	=	Environment
$\rho\vec{\boldsymbol{g}}$	=	Gravitational body forces
$\vec{\boldsymbol{v}}$	=	velocity vector
k	=	Thermal conductivity

[1] Engineer, Thermal Energy Conversion Branch.
[2] Engineer, Thermal Energy Conversion Branch.
[3] Engineer, Thermal Energy Conversion Branch.

II. Introduction

Stirling convertors are being operated by the NASA Glenn Research Center (NASA GRC) for multiple years to demonstrate that Dynamic Radioisotope Power Systems (DRPS) are capable of providing reliable power for potential multi-year deep space missions. Currently, NASA GRC has Stirling convertor contracts with American Superconductor (AMSC) and Sunpower Incorporated for the development of the next generation of free-piston Stirling convertors for Dynamic Radioisotope Power Systems. Extensive laboratory testing is planned to assess the performance of the convertors. Techniques used to monitor Stirling convertor performance includes measurements of temperature, pressure, energy addition, and power output. Quantifying net heat input is a parameter that helps to verify convertor efficiency. However, it is difficult to directly measure net heat input to Stirling convertors. This is due to the complex geometries, and the invasive sensor integration that would be required to get data helpful in establishing net heat input.

III. Background

Designing and evaluating the performance of a Stirling convertor is a complicated task. One of the ways the task is made easier is by the design tool Sage, which can be used to size the components, evaluate configurations, and predict the performance of an entire Stirling convertor. Sage is a multi-physics tool[1], but is considered low fidelity since it contains an agreed-upon numerical error on the order of 10-20%. This is because it is a 1-Dimensional code. However, it is a multi-physics tool and is capable of providing the user with estimates of electric output (W) when supplied with parameters such as acceptor temperature, rejector temperature, piston and displacer amplitudes, frequencies, and linear alternator efficiency (among many other parameters). Once a Sage model is properly set up, it runs relatively quick (when compared to most 3-D Computational Fluid Dynamic models). Optimizing each of the components towards a program-specified design target can be performed in a reasonable amount of time. While predictions of heat distributions and convertor performance are produced quickly, parameters such as net heat input are not always easily extracted from the results of a Sage run but can be calculated externally, by hand.

The commercially available analysis tool ANSYS Fluent[2] is considered a high fidelity tool, and can provide a great deal of detail regarding the fluid mechanics and heat transfer flow physics in various locations in the convertor. It enables one to calculate net heat input and reveals the temperature distribution throughout the convertor. To gain confidence in the Sage result, a Computational Fluid Dynamics (CFD) model was utilized using the ANSYS Fluent code. However, in the absence of the extra Fluent modules which make available the ability to calculate other types of physics, the ANSYS Fluent model used here was limited by not being capable of connecting the effects of the Stirling cycle to the linear alternator, or the linear alternator to the electrical output of the convertor. Even if these modules are activated, the additional time needed to obtain a transient Fluent solution becomes significant.

At various stages, numerical simulations are run and compared with each other, and with experimental data. At the time this paper was written, laboratory testing of the Sunpower Stirling convertor had begun in the NASA Glenn Stirling Research Lab (NASA GRC SRL). This particular convertor is referred to as the Sunpower Robust Stirling Convertor (SRSC), which is based on earlier Advanced Stirling Convertor (ASC) designs. Later simulations in this publication utilized lab-measured gross heat input and boundary temperatures as boundary conditions for the simulations.

IV. Modeling

The generalized schematic of a < 100 watt free-piston Stirling convertor is shown in Figure 1. The components encapsulated by the heater head on the left (displacer, heat exchangers, and the Stirling working spaces) produces the Stirling cycle. The components encapsulated by the pressure vessel (on the right) include the alternator, spring, flex rod, magnet, coil, and the gas bearing-equipped piston. Piston and magnet motion adjacent to a stationary coil contributes to the production of the electric power from the device. As stated earlier, Sage models the entire convertor. The ANSYS Fluent models in this document will include the heater head and the components encapsulated by the heater head, while excluding the remainder of the convertor components. The intent is to book-keep hot section heat.

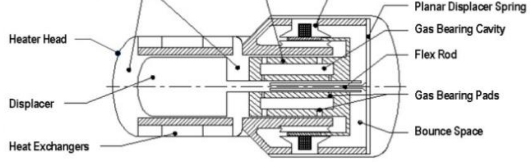

Fig. 1 Generalized Schematic of a Stirling Convertor.

The original and modified versions of the SRSC are shown in Figure 2. Figure 2(a) shows the complete geometry while Figure 2(b) shows the truncated geometry which is used primarily for the ANSYS Fluent models. The internal geometry is not shown because it is protected information. All of the simulated results in this document will only show the external convertor surfaces although the internal components were modeled.

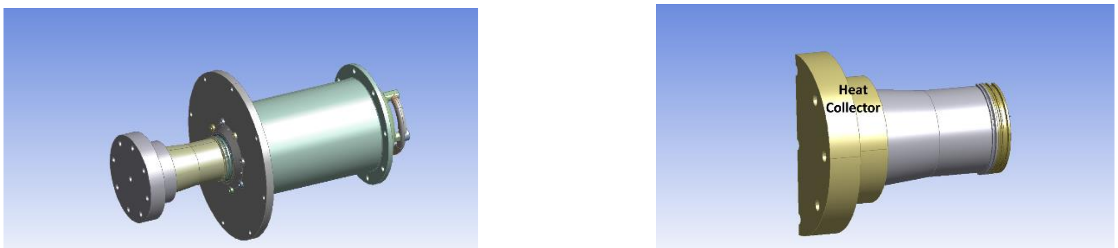

(a) Complete SRSC Geometry (b) Truncated SRSC

Fig. 2 Geometry of the Sunpower Robust Stirling Convertor (SRSC).

A. SAGE

The design tool Sage was used to optimize the SRSC based on an in-line piston-displacer configuration. Each block making up the convertor has its own characteristics and utilizes specific equations to perform transient calculations. A source pressure is applied to the bounce space adjacent to the piston, and the calculations start there, allowing the gas to propagate throughout the rest of the convertor. Blocks include solid surfaces such as iso-thermal, thick surface, and rigorous surfaces. Thick and rigorous surfaces are quasi-adiabatic surfaces, meaning they produce zero mean heat flow, but non-zero instantaneous heat flow. They are assembled with their gas duct counterparts to mimic the expected interaction of the convertor components. They are connected for observing energy transfer, and solved in series until all energy flows completely converge. Each block has other unique parameters (depending on the type of block) that must be set prior to generating a solution. The governing equations used in Sage are nonstandard relative to the computational fluid dynamics approach because they are specifically designed for one-dimensional internal flows with space- and time-variable flow area. The starting point of the formulation is the Navier-Stokes equations in integral form, but body forces are neglected and the convention stipulating that the control volume is fixed, is relaxed. The governing equations of fluid mechanics and heat transfer used by Sage include continuity (conservation of mass).

$$\frac{d}{dt}\int_v \rho dv + \int_s \rho \boldsymbol{n} \cdot \boldsymbol{V_r} ds = 0 \tag{1}$$

the momentum equations (conservation of momentum)

$$\frac{d}{dt}\int_v \rho \boldsymbol{V} dv + \int_s [(\boldsymbol{n} \cdot \boldsymbol{V_r})\rho \boldsymbol{V} - \boldsymbol{n\sigma}] ds = 0 \tag{2}$$

and the energy equation (conservation of energy)

$$\frac{d}{dt}\int_v \rho e dv + \int_s \boldsymbol{n} \cdot (\rho e \boldsymbol{V_r} - \boldsymbol{\sigma V} - \boldsymbol{q}) ds = 0 \tag{3}$$

B. ANSYS Fluent

Compared to the Sage solver, the Fluent solver contains a system of equations that govern multi-dimensional heat transfer and fluid mechanics (Navier-Stokes equations). Although the Fluent model has volumes representing metals and fluids, the more robust calculations would be performed in the dynamic fluid volumes which ultimately produces indicated or PV power from the dynamic volumes. In this case, the Fluent model is a reduced version of the complete convertor as there are some components (i.e. bounce spaces, displacer springs) that are not included. Also, it is being run steady (no motion). This helps reduce the runtime for the CFD model.

The solver ANSYS **Fluent** solves the governing equations of fluid mechanics and heat transfer. The governing equations used by Fluent include the continuity (conservation of mass)

$$\frac{\partial \rho}{\partial t} + \nabla \cdot (\rho \vec{v}) = 0 \tag{4}$$

the momentum equations (conservation of momentum)

$$\frac{\partial}{\partial t}(\rho\vec{v}) + \nabla \cdot (\rho\vec{v}\vec{v}) = -\nabla p + \nabla \cdot (\bar{\bar{\tau}}) + \rho\vec{g} \quad (5)$$

and the energy equation (conservation of energy)

$$\frac{\partial}{\partial t}(\rho E) + \nabla \cdot \left(\vec{v}(\rho E + p)\right) = \nabla \cdot \left(\mathrm{k}\nabla T + (\bar{\bar{\tau}} \cdot \vec{v})\right) \quad (6)$$

The steady versions of these equations are being used to generate predictive quantities of heat transfer and temperature distributions throughout the device.

C. Solution Scheme

The Navier-Stokes system of equations used in Fluent are solved using a segregated pressure-based finite-volume approach. The SIMPLE algorithm is used to solve the system of equations. The algebraic multigrid solver[3] (AMG) is used to solve the pressure-correction equation. In the AMG Solver, the V-cycle was applied to all equations except the energy equation. The energy equation used the F-cycle. BCSTAB (*Bi-Conjugate gradient STABilized method*) is also applied. A user-defined C++ program is used to define and apply the perimeter temperature boundary conditions

Radiation heat transfer is activated on the volume surfaces encapsulated by the displacer, only. Calculating radiation starts with the radiative transfer equation (RTE) for an absorbing, emitting and scattering medium at position $\vec{r}$ in the direction $\vec{s}$. The RTE is

$$\frac{dI(\vec{r},\vec{s})}{ds} + (a + \sigma_s)I(\vec{r},\vec{s}) = an^2\frac{\sigma T^4}{\pi} + \frac{\sigma_{\sigma s}}{4\pi}\int_0^{4\pi} I(\vec{r},\vec{s}')\Phi(\vec{s},\vec{s}')\,d\Omega' \quad (7)$$

where

$\vec{r}$ = position vector
$\vec{s}$ = direction vector
$\vec{s}'$ = scattering direction vector
s = path length
a = absorption coefficient
n = scattering coefficient
σ = Stefan-Boltzmann constant (5.669x10-8 W/m2-K4)
I = radiation intensity, which depends on position ($\vec{r}$) and direction ($\vec{s}$)
Φ = phase function
Ω' = solid angle

When selecting a radiation model within ANSYS Fluent, the Discrete Ordinances (DO) radiation model was chosen. The DO model considers the RTE in the direction $\vec{s}$ as a field equation. Instead of ray tracing, the DO model transforms the RTE into transport equations for radiation intensity in the spatial coordinates (x, y, z). The DO model solves for as many transport equations as there are in directions $\vec{s}$. The DO application of the RTE equation is shown below as

$$\nabla * (I(\vec{r},\vec{s})\vec{s}) + (a + \sigma_s)I(\vec{r},\vec{s}) = an^2\frac{\sigma T^4}{\pi} + \frac{\sigma_{\sigma s}}{4\pi}\int_0^{4\pi} I(\vec{r},\vec{s}')\Phi(\vec{s},\vec{s}')\,d\Omega' \quad (8)$$

Default values of the absorption (0) and scattering (1) coefficients were used. The emissivity of all of the displacer-encapsulated internal surfaces was set to 0.18.

D. Convertor-Only Simulation Results

Prior to receipt of the SRSC convertor, hand calculations and ANSYS models were used to obtain an estimate of thermal losses at the cold-end. The targeted hot-end temperature was ~699 °C, and the cold-end temperature was adjusted within a range of 20 – 175 °C. The resulting predictions are shown in Figure 3. GRC-1D is a series of hand calculations using Fourier's law for an isotropic medium. It is applied to all of the material components encapsulated by the heater head (including the heater head), a summed for various cold-end temperatures. Predictions using ANSYS

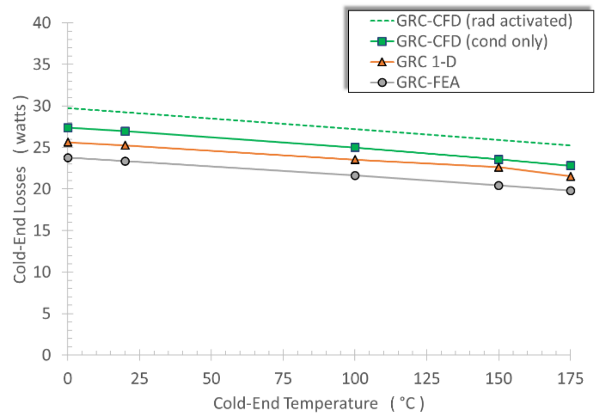

Fig. 3 Cold-end losses as a function of cold-end temperature

Mechanical (GRC FEA) and 1D calculations were used to help guide and troubleshoot the CFD model early on. The CFD model was used later for predicting final net heat input values.

V. Results

The SRSC convertor was received in an insulation and heating package. It is shown below in Figure 4. At this stage, the heater head and its encapsulated internal components are included in the ANSYS Fluent model, and the insulation and heater packages have been added. A photo of the test configuration and the instrumented test article is shown in Figure 4(a). The materials that make up the insulation and heating packages are labelled and shown in Figure 4(b).

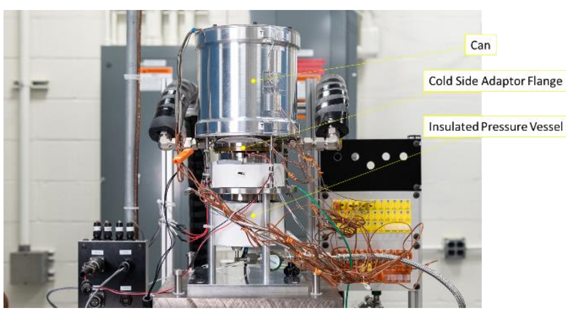

(a) SRSC on test stand in NASA GRC SRL

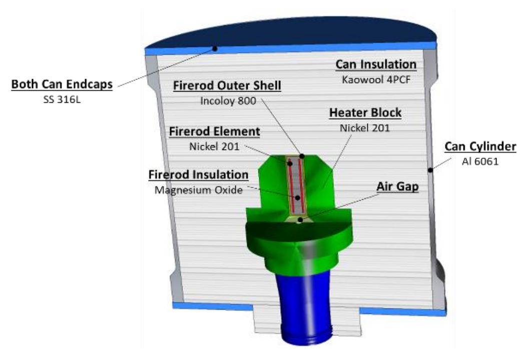

(b) Fluent geometry of insulated truncated SRSC

Fig. 4 SRSC convertor.

The can inner insulation is Kaowool, which is a porous, ceramic, low thermal conductivity insulation. When used in a vacuum, the Kaowool thermal conductivity is, most likely, as reported by the manufacturer. However, it has pore pockets which contains air when used in the laboratory. As a result, there is additional conduction (air and Kaowool) and radiation occurring as it performs its function, making it less efficient than if it were used in a vacuum. This implies that the effective thermal conductivity (that would include air and Kaowool conduction and radiation) will be higher than the manufacturer-reported thermal conductivity. An adjustment to obtain the effective thermal conductivity becomes very important since the Kaowool insulation does not participate in the radiation calculations.

A. Insulation Loss

Upon receipt of the convertors, a series of Insulation Loss tests were performed on the non-operating convertors. Heat is applied to the instrumented test article (shown in Figure 4a), and temperatures are collected. Figure 5 has labels that indicate where applied heat (GHI) and measured data is collected. This data is used with the Fluent model to quantity the effective thermal conductivity of the Kaowool and how it should be adjusted to produce the temperature distribution that was measured during testing.

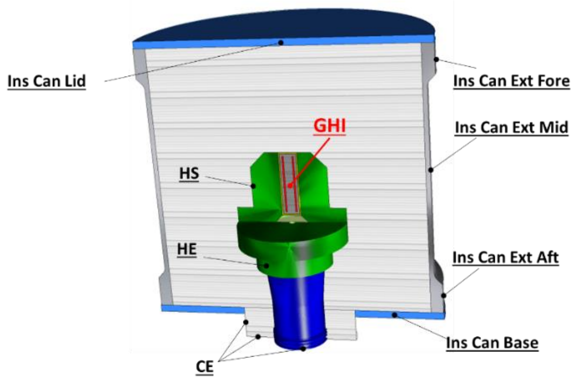

Fig. 5 Fluent model and corresponding locations of measured data.

Some of the measured data is shown in Table 1. The perimeter temperatures are applied to the Fluent model and the GHI is applied as a heat source to the heater element in the model. Using the manufacturer-supplied thermal conductivity for Kaowool 4pcf as a starting point, calculations were performed and the hot-end temperature was monitored. Initially, the hot-end temperature was much higher than the target 700.4 C, which was measured. The Kaowool thermal conductivity was increased slightly and re-run. This process was repeated until the predicted hot-end temperature was within 2 degrees of the measured hot-end temperature for this condition.

Table 1. Measured Insulation Loss points for SRSC #1.

Convertor #	Point #	Ins Can Lid C	Ins Can Ext Fore C	Ins Can Ext Mid C	Ins Can Ext Aft C	Ins Can Base C	GHI W_{th}	Avg Hot-End C	Avg HS Temp C	Avg CE Temp C
SRSC-1	S1	*43.4*	*43.2*	*43.9*	*45.1*	*51.2*	*24.1*	*300.0*	*312.5*	*100.9*
SRSC-1	S2	*59.1*	*55.9*	*56.7*	*57.9*	*65.2*	*56.6*	*501.1*	*522.8*	*100.6*
SRSC-1	**S3**	***83.6***	***76.1***	***77.0***	***78.0***	***87.2***	***104.7***	***700.4***	***730.9***	***100.1***
SRSC-1	S3L	*79.5*	*70.4*	*70.8*	*70.7*	*76.0*	*107.9*	*700.2*	*731.4*	*20.2*
SRSC-1	S3H	*85.8*	*79.7*	*81.0*	*83.0*	*95.7*	*102.4*	*700.3*	*729.0*	*150.0*

Figure 6 is a plot of temperature contours. The predicted hot-end (HE) temperature was 1.9 degrees higher than what was measured. In order for this hot-end temperature prediction to be established, the effective thermal conductivity of Kaowool had to be increased 11.1% above that supplied by the manufacturer. This adjustment is expected to be appropriate for similar temperature gradients that bound the Kaowool insulation.

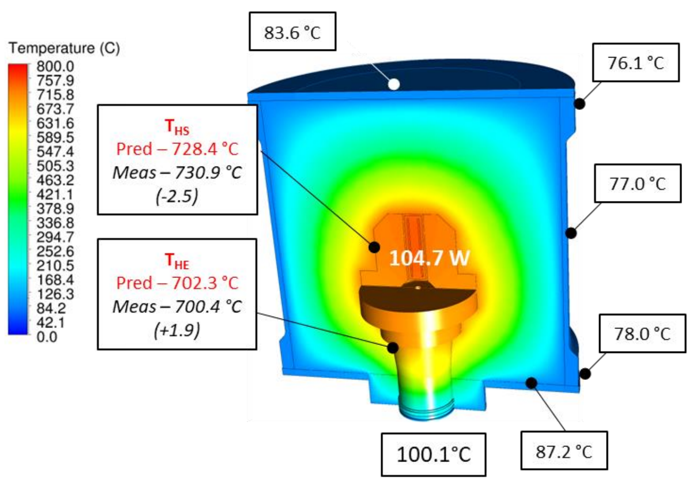

Fig. 6 Insulation Loss Temperature contour predictions with a 100 °C cold-end temperature.

For this Insulation Loss case with applied boundary conditions (S3), the details are shown in Table 1. Predicted cold-end losses out of the convertor are 25 watts while the heat loss to the environment is 79.7 watts, as seen in Table 2.

Table 2. Insulation Loss heat transfer predictions for SRSC # 1 with a 100 °C cold-end temperature.

		TARGET		SRSC-1 *(S3)* *radiation activated*	
Q_{HTR}	*(W)*			104.7	
T_{HTR}	*(C, K)*	730.9	1,003.9	728.4	1,001.4
T_{HE}	*(C, K)*	700.4	973.4	702.3	975.3
T_{CE}	*(C, K)*	100.1	373.1	100.1	373.1
Q_{CE}	*(W)*			25.0	
Q_{ENV}	*(W)*			79.7	
Q_{TOT}	*(W)*			104.7	

B. Simulated Operation

Once Insulation Loss (non-operational) tests are completed, a series of operational tests are performed. The data measured (and collected) was used as boundary conditions for the Fluent model. The operational points are shown in Table 3. More data was collected, but only the data needed for the simulations are shown in this table.

Table 3. Measured operation points for SRSC #1.

Convertor #	Point #	Ins Can Lid *C*	Ins Can Ext Fore *C*	Ins Can Ext Mid *C*	Ins Can Ext Aft *C*	Ins Can Base *C*	GHI W_{th}	Avg Hot-End *C*	Avg HS Temp *C*	Avg CE Temp *C*
SRSC-1	1a	91.4	78.1	78.0	77.0	81.3	357.0	700.4	813.9	21.1
SRSC-1	1b	93.5	79.8	79.6	78.5	82.1	381.4	700.6	822.7	20.8
SRSC-1	1c	85.9	75.8	75.9	75.4	79.9	182.4	700.7	757.6	20.1
SRSC-1	2a	**93.0**	**82.1**	**82.4**	**82.8**	**90.2**	**310.1**	**700.3**	**797.2**	**100.1**
SRSC-1	2b	94.8	82.6	83.0	83.1	90.5	357.0	700.2	813.5	99.9
SRSC-1	2c	89.6	81.0	81.6	82.1	88.2	184.3	700.7	757.6	100.2
SRSC-1	3a	99.1	90.1	91.1	92.8	105.1	331.8	699.8	804.3	175.0
SRSC-1	3b	94.9	89.9	91.3	93.9	106.6	182.7	700.1	756.1	175.2

The Insulation Loss tests for boundary condition S3 has the same cold-end temperature as that from operational point 2A, and is set in the model. Operational point 2A also has similar perimeter temperatures, which are applied to the model. In addition, the effective thermal conductivity is set to be 11.1% above the manufacturer-supplied temperature-dependent definition.

Because the cases are operational, a higher GHI is necessary. In the convertor, some of the GHI is converted to PV power. While this conversion doesn't occur in the steady model, it is thermally accounted for by extracting heat

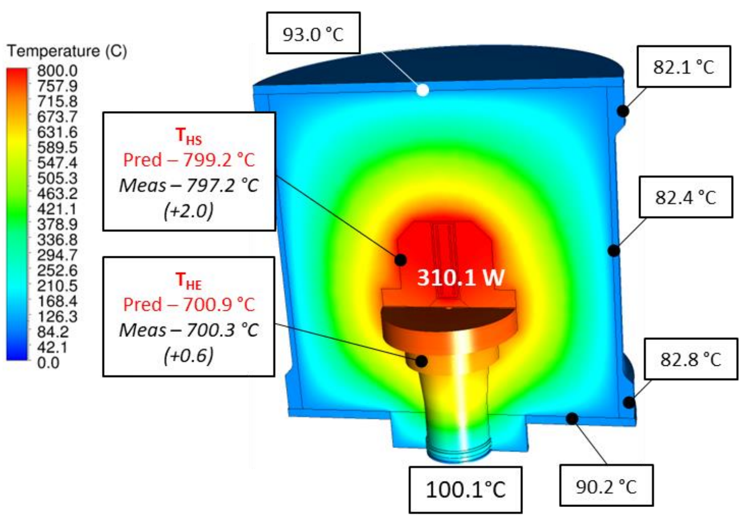

Fig. 7 Operating point (2A) temperature contour predictions with a 100 °C cold-end temperature.

from the Expansion Space (ES). At the beginning of this calculation, no heat is extracted via the ES and the resulting predicted hot-end temperature is very high. As the quantity of heat extracted from the ES is increased, the hot-end temperature goes down. The results of these calculations are shown in Table 4.

Table 4. Operating point (2A) heat transfer predictions for SRSC # 1 with a 100 °C cold-end temperature.

		TARGET		SRSC-1 (2a)
				Radiation Activated
Q_{HTR}	*(W)*			**310.1**
T_{HTR}	*(C, K)*	**797.2**	**1,070.2**	1,072.2
T_{HE}	*(C, K)*	**700.3**	**973.3**	973.9
T_{CE}	*(C, K)*	**100.1**	**373.1**	373.1
Q_{CE}	*(W)*			**24.2**
Q_{ENV}	*(W)*			**89.4**
Q_{ES}	*(W)*			**196.5**
Q_{TOT}	*(W)*			**310.1**
NHI	*(W)*			***220.7***

For operating point 2A, the predicted hot-end temperature was within 0.6 degrees of measured data. To get this close to the measured hot-end temperature, 196.5 watts of heat was extracted from the ES volume. This left 24.2 watts for cold-end losses and 89.4 watts going to the environment. The Net Heat Input (NHI) is the sum of the cold-end losses and the heat extracted through the Expansion Space (ES), which is 220.7 watts.

C. Summary

Most of the conditions run in the lab were completed. The operating point conditions calculated are shown in Table 5. The NHI (Net Heat Input) can be used to calculate the convertor operating efficiency via *Desired Output*/*Required Input,* where the power output is the desired output and NHI is the required input.

Table 5. Summary of predicted operating point results.

		SRSC 1				
		1A	*2A*	*2B*	*2C*	*3A*
Target T_{HTR}	*(K)*	*1,086.9*	*1,070.2*	*1,086.5*	*1,030.6*	*1,077.3*
Target T_{HE}	*(K)*	*973.4*	*973.3*	*973.2*	*973.7*	*972.8*
Target T_{CE}	*(K)*	*294.1*	*373.1*	*372.9*	*373.2*	*448.0*
Q_{HTR}	*(W)*	**357.0**	**310.1**	**357.0**	**184.3**	**331.8**
T_{HTR}	*(K)*	1,088.1	1,072.2	1,088.7	1,030.3	1,079.2
T_{HE}	*(K)*	973.3	973.9	973.7	973.7	973.0
T_{CE}	*(K)*	294.1	373.1	372.9	373.2	448.0
Q_{CE}	*(W)*	**26.2**	**24.2**	**24.0**	**24.6**	**21.6**
Q_{ENV}	*(W)*	**92.8**	**89.4**	**91.8**	**83.1**	**89.6**
Q_{ESD}	*(W)*	**238.0**	**196.5**	**241.2**	**76.6**	**220.6**
Q_{TOT}	*(W)*	**357.0**	**310.1**	**357.0**	**184.3**	**331.8**
NHI	*(W)*	***264.2***	***220.7***	***265.2***	***101.2***	***242.2***

VI. Conclusions

An overview of the Insulation Loss predictions is shown in Figure 8. It shows that parasitic losses (environmental and cold-end) are linear with increasing GHI, as long as the fixed cold-end temperature remains constant. This

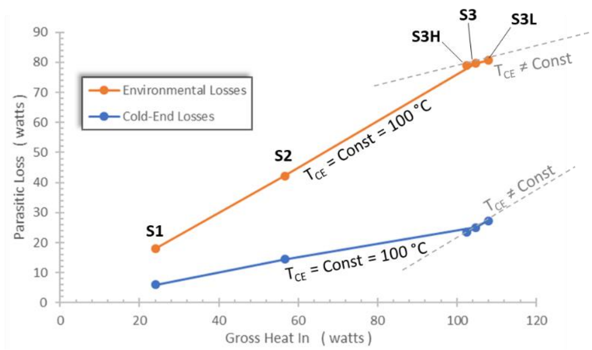

Fig. 8 Summary of Insulation Loss predictions.

predictable behavior makes it possible to program the data acquisition system to provides estimates of the carious parasitic losses based on the input GHI during testing.

Figure 9 shows a summary of some of the operating points that were simulated. This plot shows that for the cases run, NHI is a linear function of GHI. The operating points have common hot-end temperatures. More simulations would need to be performed to see if the linear relation remains when dynamic amplitudes vary.

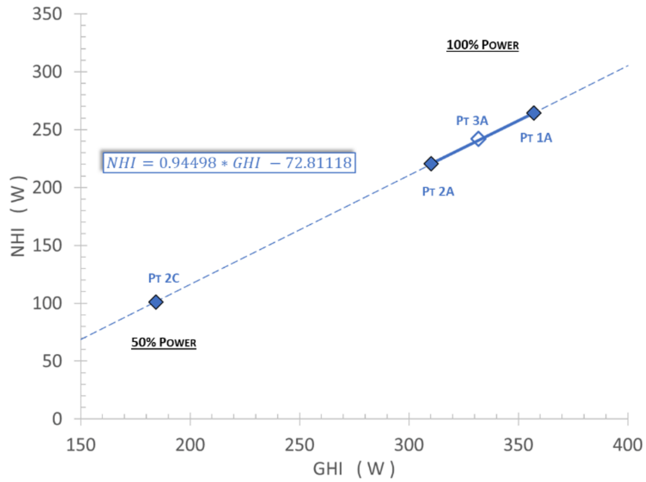

Fig. 9 Summary of operating point predictions.

A comparison of Sage versus Fluent is shown below in Table 6. There is a level of comfort with the closeness of the results. In addition, the ANSYS Fluent results provides extra detail that is not available with Sage. Numerous future calculations are planned to explore the limits of useability and usefulness of the Fluent solver for application to Stirling convertors.

Table 6. Comparison of Sage vs Fluent results.

		SRSC-1 (2a)	
		Sage	*ANSYS Fluent*
Q_{HTR}	(W)	**311.0**	**310.1**
Q_{CE}	(W)	[redacted]	**24.2**
Q_{ENV}	(W)	**88.0**	**89.4**
$Q_{PARASITIC}$	(W)	[redacted]	**113.6**
NHI	*(W)*	***223.0***	***220.7***

\

Appendix

In the main body of this document, the procedure was described and presented for a single pair of boundary (one Insulation Loss and one operational). Additional data from other predictions are being provided in this appendix.

The thermal conductivity of Kaowool is shown in the figure below. Adjustments were made to the nominal value as the calculations required. For each adjustment, a curve-fit equation was generated for input into ANSYS Fluent.

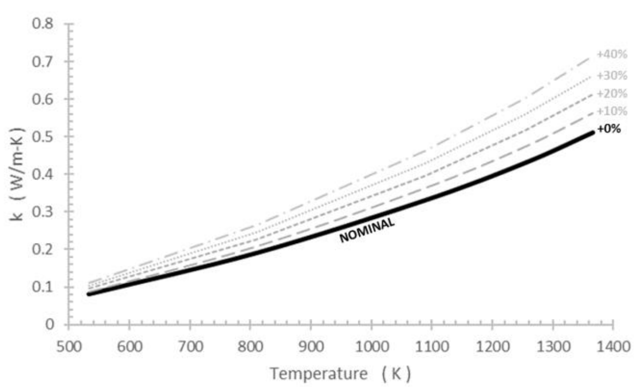

Figure 10. Thermal conductivity of Kaowool 4PCF.

Generated heat in the model is produced via heat generation by a firerod in the Fluent model. A picture of the firerod is shown in the figure below. The volume of the nickel heating element (shown in red) is calculated. The desired gross heat input is divided by the heating element volume to produce a heat generation rate (W/m^3). This is then input into Fluent to generate the model's heat.

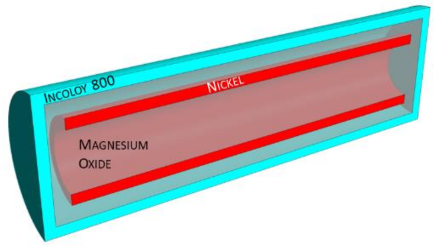

Figure 11. Heat generating firerod in the computational model.

All of the cases calculated were done with the radiation model de-activated, then activated. This was done to observe the effect of including radiation. In every case, the convertor cold-end losses increased by ~2 watts when the radiation model was activated.

The insulation loss simulations were used to determine the factor to applied to the nominal Kaowool thermal conductivity. This differed when the radiation model was de-activated or activated. The collection of Kaowool adjustments are shown in the figure below.

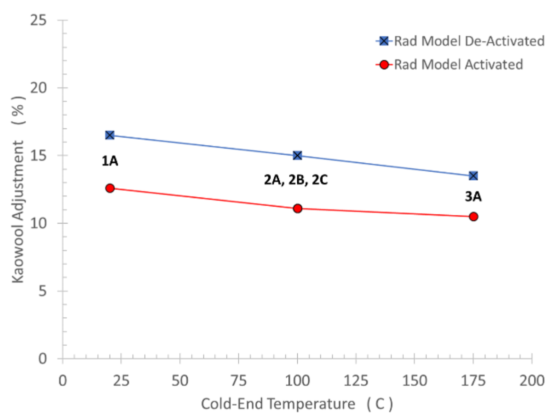

Figure 12. Kaowool adjustments when radiation model is de-activated and activated.

In the following tables, the results for the operating point conditions are shown. Above each column, the Kaowool adjustment is shown which differs whether the radiation model is de-activated or activated.

Table 7. Operating Condition 1A.

		TARGET		SRSC-1 (1a)	
				+16.5%	*+12.6%*
				Conduction Only	*Radiation Activated*
Q_{HTR}	*(W)*			**357.0**	**357.0**
T_{HTR}	*(C, K)*	**813.9**	**1,086.9**	1,087.8	1,088.1
T_{HE}	*(C, K)*	**700.4**	**973.4**	973.6	973.3
T_{CE}	*(C, K)*	**21.1**	**294.1**	294.1	294.1
Q_{CE}	*(W)*			**24.5**	**26.2**
Q_{ENV}	*(W)*			**96.0**	**92.8**
Q_{ESD}	*(W)*			**236.5**	**238.0**
Q_{TOT}	*(W)*			**357.0**	**357.0**
NHI	*(W)*			***261.0***	***264.2***

Table 8. Operating Condition 2A.

+15.0% +11.1%

		TARGET		SRSC-1 (2a)	
				Conduction Only	*Radiation Activated*
Q_{HTR}	*(W)*			**310.1**	**310.1**
T_{HTR}	*(C, K)*	**797.2**	**1,070.2**	1,070.8	1,072.2
T_{HE}	*(C, K)*	**700.3**	**973.3**	973.0	973.9
T_{CE}	*(C, K)*	**100.1**	**373.1**	373.1	373.1
Q_{CE}	*(W)*			**22.3**	**24.2**
Q_{ENV}	*(W)*			**92.3**	**89.4**
Q_{ESD}	*(W)*			**195.5**	**196.5**
Q_{TOT}	*(W)*			**310.1**	**310.1**
NHI	*(W)*			***217.8***	***220.7***

Table 9. Operating Condition 2B.

+15.0% +11.1%

		TARGET		SRSC-1 (2b)	
				Conduction Only	*Radiation Activated*
Q_{HTR}	*(W)*			**357.0**	**357.0**
T_{HTR}	*(C, K)*	**813.5**	**1,086.5**	1,087.9	1,088.7
T_{HE}	*(C, K)*	**700.2**	**973.2**	973.4	973.7
T_{CE}	*(C, K)*	**99.9**	**372.9**	372.9	372.9
Q_{CE}	*(W)*			**22.2**	**24.0**
Q_{ENV}	*(W)*			**94.9**	**91.8**
Q_{ESD}	*(W)*			**239.9**	**241.2**
Q_{TOT}	*(W)*			**357.0**	**357.0**
NHI	*(W)*			***262.1***	***265.2***

Table 10. Operating Condition 2C.

+15.0% 11.1%

		TARGET		SRSC-1 (2c)	
				Conduction Only	*Radiation Activated*
Q_{HTR}	*(W)*			**184.3**	**184.3**
T_{HTR}	*(C, K)*	**757.6**	**1,030.6**	1,029.7	1,030.3
T_{HE}	*(C, K)*	**700.7**	**973.7**	973.7	973.7
T_{CE}	*(C, K)*	**100.2**	**373.2**	373.2	373.2
Q_{CE}	*(W)*			**22.7**	**24.6**
Q_{ENV}	*(W)*			**86.0**	**83.1**
Q_{ESD}	*(W)*			**75.6**	**76.6**
Q_{TOT}	*(W)*			**184.3**	**184.3**
NHI	*(W)*			***98.3***	***101.2***

Table 11. Operating Condition 3A.

+13.5% 10.5%

		TARGET		SRSC-1 (3a)	
				Conduction Only	*Radiation Activated*
Q_{HTR}	*(W)*			**331.8**	**331.8**
T_{HTR}	*(C, K)*	**804.3**	**1,077.3**	1,078.7	1,079.2
T_{HE}	*(C, K)*	**699.8**	**972.8**	972.8	973.0
T_{CE}	*(C, K)*	**175.0**	**448.0**	448.0	448.0
Q_{CE}	*(W)*			**19.9**	**21.6**
Q_{ENV}	*(W)*			**92.0**	**89.6**
Q_{ESD}	*(W)*			**220.0**	**220.6**
Q_{TOT}	*(W)*			**331.8**	**331.8**
NHI	*(W)*			***239.9***	***242.2***

Acknowledgements

This work is funded through the NASA Science Mission Directorate and the Radioisotope Power Systems Program Office. The author wishes to acknowledge Nicholas Schifer and Luis Rodriguez for the numerous multi-physics discussions, geometry definitions, and experimental data399339 that were provided. Any opinions, findings, conclusions, or recommendations expressed in this article are those of the author and do not necessarily reflect the views of NASA.

References

[1] Gedeon, David. "Sage: Object Oriented Software for Stirling Machine Design," AIAA Paper 94-4106-CP. 1994. https://doi.org/10.2514/6.1994-4106.

[2] ANSYS Fluent: Fluent User's Guide, Release 18.0. Canonsburg, PA, ANSYS Inc, 2017.

[3] ANSYS Fluent: Fluent Theory Guide, Release 18.0. Canonsburg, PA, ANSYS Inc, 2017.